JOURNAL OF AIRCRAFT
Vol. 35, No. 2, March–April 1998

Aerodynamic Characteristics of a Gyroplane Configuration

F. N. Coton* and L. Smrcek*
University of Glasgow, Glasgow G12 8QQ, Scotland, United Kingdom
and
Z. Pátek†
Aeronautical Research and Test Institute, Beranovych 130, 199 05 Prague, Czech Republic

This paper describes the wind-tunnel testing of a scale model gyroplane in the 3-m Low-Speed Wind Tunnel at the Aeronautical Research and Test Institute, Prague. These tests were conducted by the University of Glasgow as part of a U.K. Civil Aviation Authority funded research program into gyroplane airworthiness and flight safety. The wind-tunnel test program had two distinct aims. The first was to provide basic aerodynamic data on the effects of configurational characteristics of a gyroplane with a view to assessing the degree to which specific design features such as cowlings and tailplanes are beneficial to gyroplane performance. Secondly, it was intended to provide aerodynamic data for input to mathematical models to validate parametric studies of static and dynamic stability carried out as part of the overall research program. The results from the wind-tunnel test program show that the aerodynamic characteristics of the vehicle are generally benign, although the cowling, which provides the pilot with protection from the elements, has a destabilizing influence under certain conditions.

Nomenclature

Cl = rolling moment coefficient
Cm = pitching moment coefficient
Cn = yawing moment coefficient
C_T = propeller thrust coefficient, $T/\rho V^2 d^2$
Cx = axial force coefficient
Cy = side force coefficient
Cz = normal force coefficient
d = propeller diameter
R = rotor radius
T = propeller thrust
V_w = wind speed
α = angle of attack
β = sideslip angle
δ_r = rudder deflection angle
ρ = air density

Introduction

THE autogyro, or gyroplane, has been used for recreational and sport flying since before World War II. Despite this, however, gyroplanes have failed to establish a permanent foothold for either military or commercial applications. As a result, the machines have not been subject to the constant research and development focused on other flight vehicles. Consequently, the gyroplane of today has changed little from its prewar counterpart and, more importantly, lacks the technical backup that would normally be attributable to a modern-day aircraft. In light of this, and the recent accident rate experienced by the aircraft, a study of gyroplane flight mechanics is overdue. In the United Kingdom alone, there were six fatal gyroplane accidents in the 1989–1991 period.[1] This viewpoint is further reinforced by the continued popularity of gyroplanes with recreational flyers and also the potential these machines have in providing low-cost flight data for rotorcraft modeling applications.[2]

The main body of research on gyroplane configurations dates from before 1940. Although initial studies concentrated on the theoretical development of the vehicle,[3,4] subsequent investigations addressed practical issues such as aerodynamics[5–10] and even rotor structural behavior.[11] Indeed, by the late 1930s, a sound basis existed for the future examination of the stability and control of these vehicles. Unfortunately, commercial and military interest in gyroplanes waned with the arrival of the helicopter in 1939 and, as a result, very little postwar research has been documented.

A major program of research to examine the stability and controllability of gyroplanes, to develop a computational tool that could be used to support studies into gyroplane stability, and to support the development of a new airworthiness design standard in the United Kingdom[12] has been undertaken. The computational tool is described elsewhere.[13]

This paper presents results of an experimental program to identify the aerodynamic effects of the principal aircraft features such as a cowling and tail surfaces.

Configurations

The wide variety of gyroplane configurations currently in service made it difficult to select only one as a suitable basis for the wind-tunnel test program. Clearly, however, there are some key design features which, if not standard to each vehicle, characterize the range of geometries. In particular, a horizontal tailplane is common to most aircraft, and a front cowling, to protect and streamline the pilot, is a feature of many commercial designs. Together with the body of the pilot, the inclusion of these features dominate the geometry of the vehicle. For this reason, a model, which allowed for the attachment and removal of both a front cowling and horizontal tail, was constructed. It was then possible to use this model to study a range of possible geometries.

The actual wind-tunnel model was a one-third scale representation of a VPM-M14 gyroplane. This aircraft has a very large front cowling and is capable of accommodating a pilot and passenger in tandem. It also has an unusually large horizontal tail with vertical end plates. The relative size of both the cowling and tail was deemed to be an advantage in this case as it would serve to enhance the aerodynamic effect re-

Presented as Paper 96-4.3.4 at the 20th Congress of the International Council of the Aeronautical Sciences, Sorrento, Italy, Sept. 8–13, 1996; received Nov. 26, 1996; revision received Sept. 2, 1997; accepted for publication Sept. 23, 1997.

*Senior Lecturer, Department of Aerospace Engineering.
†Head of Low Speed Aerodynamics.

sulting from their addition or removal from the configuration. A diagram of the model, indicating its overall dimensions, is shown in Fig. 1.

The basic model frame was constructed from a metal box-section on which a water-cooled electric motor was mounted. This motor was connected by a toothed-belt to the propeller drive system. The removable tailplane assembly and the representations of the aircraft wheels and wheel covers were fabricated in aluminum. The front cowling was made from glass fiber. In addition to the basic features of the aircraft, it was necessary to model the aerodynamic effect of the pilot. This was achieved by creating a scaled representation of the pilot's upper body that was mounted in an appropriate position on the model frame. The motor and its support flange were then positioned in such a way that their forward projection and cross section provided a scaled representation of the pilot's lower body when the cowling was removed.

The experimental program involved tests on four different gyroplane configurations, with the baseline being the cowling-on, tail-on configuration. The other configurations were produced by cowling-on/off and horizontal tail-on/off combinations. In addition, although not documented here, specific tests were conducted involving the extension of the tail boom and removal of the horizontal tail end plates. In each case, however, force and moment coefficients were obtained for both a power-off and a nominal criuse power-on condition. The key used to relate the results in the following figures to each of these configurations is shown in Table 1.

A total of 114 data polars were measured covering the following parameter ranges: $-40 < \alpha < 40$ deg, $-30 < \beta < 30$ deg, and $-20 < \delta_r < 20$ deg.

All tests were conducted in the absence of the main rotor because the complexity and cost of the model would have been greatly increased if the rotor had been included when it would only, at best, have been possible to achieve partial similarity with the full-scale rotor. Another reason for testing in this way lay in the intended use of the data within flight mechanics models. These models contain aerodynamic simulations of the main rotor effect, and require clean fuselage data as input. The detailed manner in which the data from the present study were integrated into the flight mechanics simulations is described in Ref. 13.

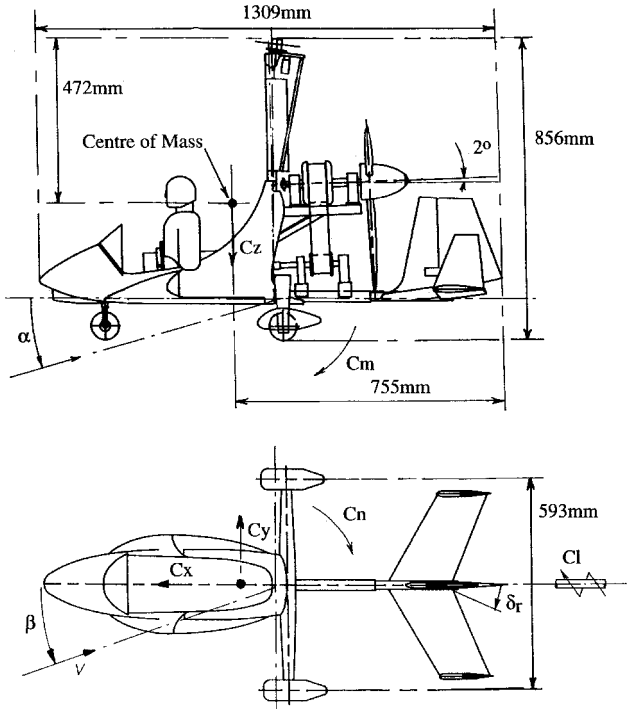

Fig. 1 Wind-tunnel model and coordinate system.

Table 1 Key to test runs

Test case	Key
Cowling on, tail on, power on	
Cowling on, tail on, power off	
Cowling off, tail on, power on	
Cowling off, tail on, power off	
Cowling on, tail off, power on	
Cowling on, tail off, power off	
Cowling off, tail off, power on	
Cowling off, tail off, power off	

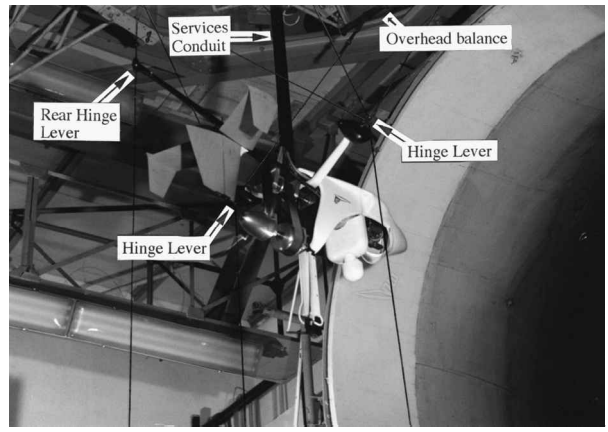

Fig. 2 Model mounting arrangement in wind tunnel.

Wind-Tunnel Test Setup

All tests were conducted in the 3-m Low-Speed Wind Tunnel of the Aeronautical Research and Test Institute (VZLU) of Prague in the Czech Republic. This institute has provided high-quality wind-tunnel facilities for the Czech aircraft industry for many years. The particular wind tunnel used in this study was an atmospheric open-section, closed-return, Gottigen-style tunnel with a maximum velocity of around 60 m/s. The average turbulence intensity in the working section was 0.3%. Forces and moments were measured on a six-component fully automatic overhead gravitational balance.

The model was mounted, as shown in Fig. 2, in inverted mode on the wind-tunnel balance by a series of connecting wires. Services to and from the motor were provided by a streamlined conduit located centrally above the model. This conduit, which was attached to the balance frame, not only provided a power supply for the model but also housed the water pipes necessary for the motor cooling system. The angle of attack and sideslip settings of the model were automatically adjusted using the balance control system. Rudder deflection was achieved manually.

The model was tested in both power-on and power-off modes. In the latter case, the propeller was removed from the model during testing. For powered tests, the thrust coefficient and advance ratio of the model propeller were matched to the level cruise performance of the full-scale gyroplane propulsion unit. The cruise thrust coefficient or the propeller was estimated from flight test data in conjunction with the available flight mechanics models. Thus, although the model was tested in the absence of the main rotor, the thrust was set to overcome the rotor drag. The value of C_T used in this case was fixed at $C_T = 0.317$. This corresponded to an increment in the Cx of 0.0516. The model propeller had a diameter exactly one-third of the full scale but was, otherwise, not geometrically similar. A stand-alone calibration for this propeller was available and an additional calibration involving measurements with the propeller attached to the gyroplane fuselage was conducted. This allowed a correction to be made for degradation of the thrust caused by interference with the fuselage. Because of the inherent limitations of scaling and the method used, it was not

Table 2 Accuracy of coefficients

Coefficient	Uncertainty
Cx	±0.0004
Cy	±0.00008
Cz	±0.0004
Cl	±0.0003
Cm	±0.0003
Cn	±0.0004

possible to match propeller torque coefficient. It should be noted here that the propeller thrust setting was held constant throughout both incidence and sideslip variations, and so the results obtained effectively represent short-term deviations from cruise. Given that the gross effect of the propeller on the flight vehicle aerodynamics was of primary interest, this was considered adequate.

All tests were conducted at a Reynolds number, based on the rotor radius, of 2.5×10^6, which corresponds to a wind-tunnel flow velocity of 31 m/s and was approximately 40% of that of the full-scale vehicle during cruise. This Reynolds number difference would be expected to have little effect on the vertical tail surfaces, which were effectively flat plates with a thickness-to-chord ratio of less than 5%. The main effect, if any, would be on the horizontal tail, which had a NACA 0012 cross section and achieved a chord Reynolds number of about 4×10^5 based on the freestream velocity. The most likely manifestation of the Reynolds number difference would be some modification of the stalling incidence of the tail and, hence, the maximum lift obtained by it. This is further complicated, however, by the close coupling of the tail and the propeller whose slipstream, under certain flight conditions, washes over the tail. Unfortunately, the constraints on the test program were such that a wind-tunnel-based investigation of the Reynolds number effect was not possible.

Presentation of Coefficient Data

The coordinate system used for all force and moment coefficients presented in the following sections is illustrated in Fig. 1. The coefficients are referenced to the c.m. of the full-scale aircraft, including rotor, when carrying a full load of fuel. In terms of model coordinates, the c.m. for the zero fuel case is approximately 1 mm further aft and 15 mm higher than the indicated position in Fig. 1. The nondimensional coefficients were calculated using the rotor radius as the basic characteristic length. Thus, for example, the normal force and pitching moment are given, respectively, by

$$Z = \tfrac{1}{2}\rho V_w^2 \pi R^2 Cz$$

$$M = \tfrac{1}{2}\rho V_w^2 \pi R^3 Cm$$

By consideration of the accuracy of the wind-tunnel balance and dynamic pressure measurement system, it was possible to determine the average uncertainty associated with each of the individual coefficients. These values are presented Table 2.

Discussion of Test Results

In this section, the main features of the results from the wind-tunnel test program are presented and analyzed. Most of the data in this paper are those obtained for powered tests, although there are selective comparisons with power-off measurements.

Normal Force Coefficient

Figure 3 presents the measured normal force coefficient variations at zero sideslip for each of the four configurations examined in the study. From Fig. 3 it is clear that, as may be expected, both the slope and magnitude of the normal force are most strongly influenced by the tailplane. It is also apparent

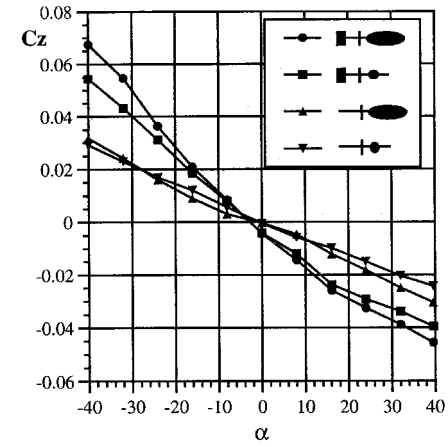

Fig. 3 Cz vs α for four gyroplane configurations ($\beta = 0$).

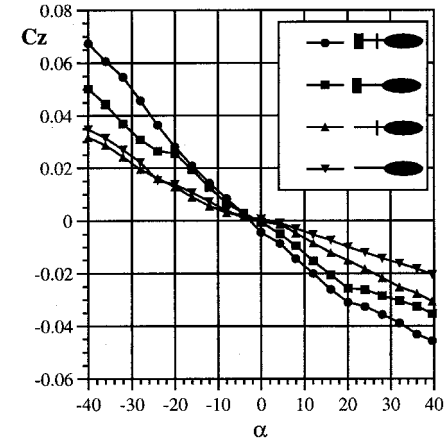

Fig. 4 Effect of power on Cz for tail-on and tail-off configurations ($\beta = 0$).

that the influence of the cowling is generally small and, at positive incidence, acts in the same sense as the tailplane. This is presumably a result of the increased wetted area presented to the flow by the significant size of the cowling. At positive incidence, the cowling increasingly obstructs the propeller inflow, thus altering the nature of the slipstream behind the propeller. This produces different effects on Cz, depending on whether the tail is on or off.

Generally, the slopes of the Cz curves are almost linear, although there is a reduction in gradient at high positive incidence when the tailplane is on. This change in gradient appears to be a result of tailplane stall as the tail moves away from the influence of the propeller slipstream. Conversely, at high negative incidence, the tail is fully enveloped by the propeller slipstream and, despite being subject to a reduced effective angle of attack, the tail generates more normal force.

The full effect of the propeller may be observed in Fig. 4, where the normal force coefficient curves measured in power-on and power-off modes are compared for two of the test configurations. At positive incidence, the propeller inflow interacts with the freestream to modify the flow over the cowling, thus increasing the normal force generated by it. On the other hand, the tail moves progressively out of the propeller slipstream and is observed to stall at the same incidence, regardless of power setting. At negative incidence, as indicated earlier, the only significant effect of the propeller is to enhance the force produced by the tail.

The effect of sideslip angle on the normal force was found to be extremely small for incidence angles less than 20 deg. At higher incidence, the angle at which tail stall occurred at both positive incidence was dependent on the sideslip angle.

This will be discussed in more detail when considering its effect on the pitching moment.

Axial Force Coefficient

As may be anticipated, the primary influence on the axial force is the thrust developed by the propeller because the propeller axis is only offset 2 deg from the axial direction. Nevertheless, there are tangible effects of configuration which, in general, produce changes in the axial force coefficient of around 4%. At high negative incidence, the change in axial force because of configuration can be more than 10% of the propeller thrust. This is illustrated in Fig. 5, where the *Cx* vs α curves for the four configurations in the power-on mode are presented.

The most significant configurational effect is the additional thrust produced by the tail at negative incidence. In this case, the magnitude of the angle of attack experienced by the tail is less than the airframe incidence because the tail lies in the slipstream of the propeller. This prevents the tail from stalling and, because of the increased dynamic pressure in the slipstream, produces more thrust at high negative incidence.

Another interesting characteristic of the tail is apparent in the variation of axial force with the sideslip angle presented in Fig. 6. This time, however, the most significant effect is observed at positive incidence and is because of the vertical tail. The variation in *Cx* occurs because the resultant velocity and angle of attack experienced by the vertical tail, and hence, the thrust developed by it, depends on the direction of the freestream and the axial and rotational velocities of the slipstream. At high incidence, the variation in onset conditions is particularly large because the strong vortex structures produced by the propeller tips are convected over the main body of the vertical tail surface.

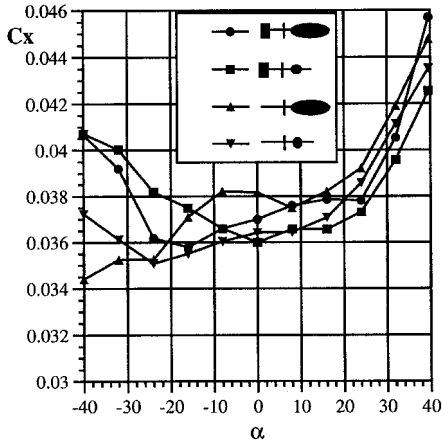

Fig. 5 Effect of gyroplane configuration on *Cx* ($\beta = 0$).

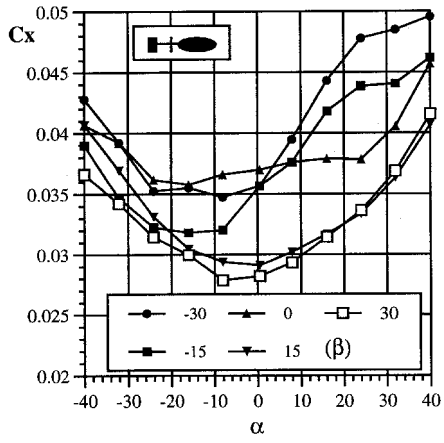

Fig. 6 Effect of sideslip angle on tangential force.

Side Force Coefficient

As shown in Fig. 7, the variation of side force with sideslip angle was found to be almost linear in the $-15 < \beta < 15$ deg range. In the case of the cowling-on, tail-on configuration, tests were conducted up to sideslip angles of 30 deg and, even there, little variation in gradient was found. The results were also relatively insensitive to model configuration and incidence setting, with the principal influence being the vertical tail. It is, however, pertinent to note that a marginal increase in side force is produced when the horizontal tail is on. This is attributable to the increased side area presented by the vertical end plates.

Pitching Moment Coefficient

The basic effects of configuration on the pitching moment are shown in Fig. 8. As may be expected, the horizontal tail acts to stabilize the flight vehicle and is effective up to its stalling incidence of around 20 deg. At negative incidence, the effects discussed earlier, in connection with the normal force, come into play and tail stall is avoided.

Perhaps the most significant feature of Fig. 8, however, is the destabilizing effect of the cowling. With the tail on, the effect of the cowling is to reduce the gradient of the *Cm* curve by almost half. Without the tail, the cowling-on configuration is marginally unstable throughout the incidence range. This result is not surprising given the large wetted area presented by the cowling and its position ahead of the c.m. Nevertheless, the magnitude of the destabilizing effect is substantial and has design implications.

Another interesting feature of the pitching moment behavior is the extent to which it is influenced by power setting. In Fig. 9, results from the baseline configuration in power-on and

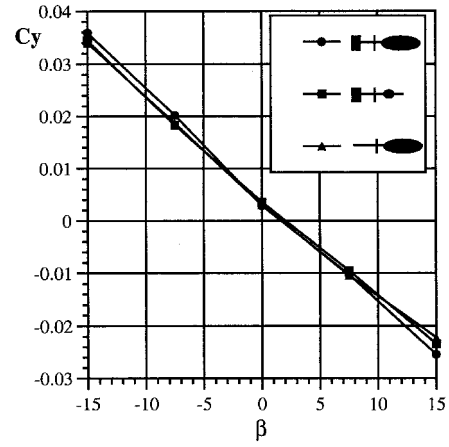

Fig. 7 Variation of sideforce with sideslip angle ($\alpha = 0$).

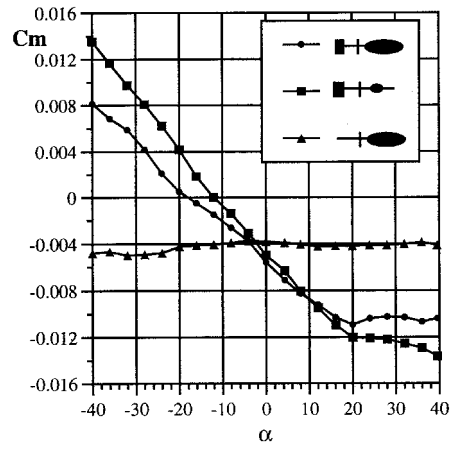

Fig. 8 Effect of configuration on *Cm* ($\beta = 0$).

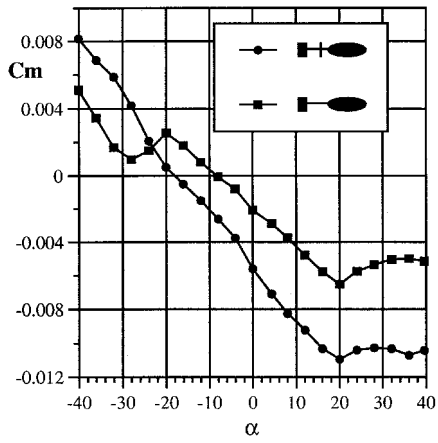

Fig. 9 Effect of power on *Cm* (β = 0).

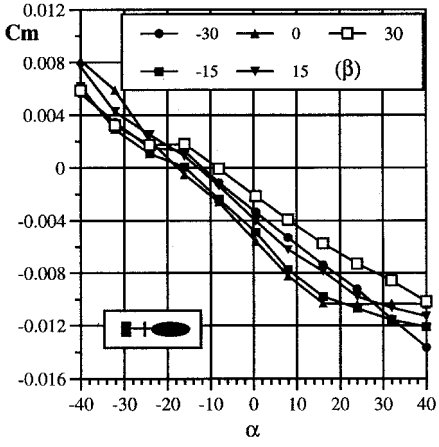

Fig. 10 Effect of sideslip angle on *Cm*.

power-off modes are compared. Clearly, the pitching moment produced by the propeller dominates the magnitude of the difference between the two curves. More subtle, however, is the effect produced by the tail at negative incidence as it enters the propeller slipstream. This increases the moment produced by the tail because of the effects of increased dynamic pressure and flow angularity, discussed in relation to the normal force. Generally, the net effect of the propwash with the tail is to produce a more linear *Cm* variation over the entire incidence range, thus enhancing stability.

The influence the propeller slipstream/tail interaction has on the pitching moment was also found to vary with sideslip angle. This variation is complex and results from two distinct aspects of the interaction. The first is the effect of the axial velocity component of the propeller slipstream which, at moderate incidence washes over the horizontal tail, enhancing the lift produced by it. This results in a nose-down pitching moment that reduces with increasing sideslip magnitude. This is illustrated in Fig. 10, where the pitching moment characteristics of the baseline configuration are presented for five sideslip angles.

A secondary effect on the tail results from the direction of rotation of the propeller slipstream. This can have a significant effect on both the direction and magnitude of the flow over the tail and, consequently, either moderates or enhances the effect of the increase in axial velocity in the slipstream. For this particular vehicle, the sense of rotation of the propeller is such that the tail experiences net downwash at positive sideslip angles, generally increasing the pitching moment.

Despite these effects, the sideslip angle produces only a small variation in the gradient of the *Cm* curves in the $-20 < \alpha < 20$ range. Outside of this incidence range, the stalling characteristics of the tail become significant and are strongly

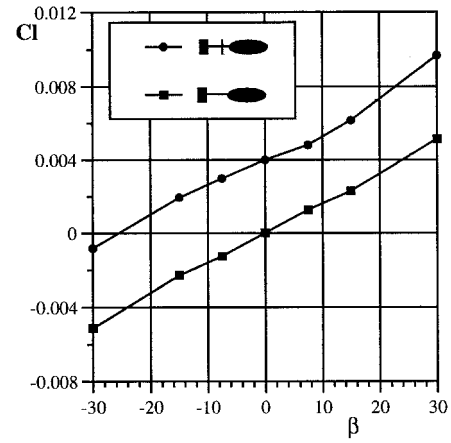

Fig. 11 Effect of power on *Cl* (α = 0).

influenced by the propeller slipstream. The manner of this interaction is strongly three dimensional but appears to be dominated, at negative incidence, by the enhanced axial velocity in the propeller slipstream. The most obvious effect of this is the prevention of stall when the gyroplane is head-on to the flow.

At positive incidence, the propeller slipstream lies above the tail and, consequently, its sense of rotation becomes a more significant factor. This is apparent in the delayed stall caused by downwash at positive sideslip angles. One interesting anomaly appears to occur at −30 deg of sideslip, where tail stall is not experienced. The reasons for this are unclear, but may be because of additional effects such as wake skew or the interaction of the slipstream with the vertical tail.

Rolling Moment Coefficient

The rolling moment produced by the gyroplane was found to be virtually insensitive to configuration and almost linear with respect to sideslip angle over the full test range. Similarly, the incidence setting also had little effect on the rolling moment.

The main influence on the rolling moment was found to be the power setting. This is shown in Fig. 11, where the variations of rolling moment with sideslip are shown for the baseline configuration at zero incidence in power-on and power-off modes. For the head-on case, the magnitude of the rolling moment is increased with the power on, as a consequence of the reaction torque and side force produced directly by the propeller. These effects may also be marginally offset by the side force produced at the tail by the rotation of the propeller slipstream. Nevertheless, the overall difference between the two cases is almost constant over the entire range of sideslip.

Yawing Moment Coefficient

The influence of gyroplane configuration on the variation of yawing moment with sideslip angle is shown in Fig. 12. Clearly, the most stable characteristic is obtained with the horizontal tail on and the cowling removed. It is pertinent to note that the horizontal tail has large end plates, which, as discussed previously, contribute to the side force and, hence, the yawing moment. In fact, from Fig. 12, it may be deduced that the effect of these surfaces to some extent offsets the destabilizing influence of the cowling.

As may be expected, the yawing moment curve is strongly influenced by the power setting, as shown in Fig. 13. This is because of two particular effects. The first of these is the restoring torque produced by the propeller when it is offset from the freestream direction. This always provides a stabilizing influence and, thus, has the effect of increasing the gradient of the curve. The second effect is the increase in side force produced at the tail because of the rotation of the propeller slipstream. This additional force always acts in the same direction,

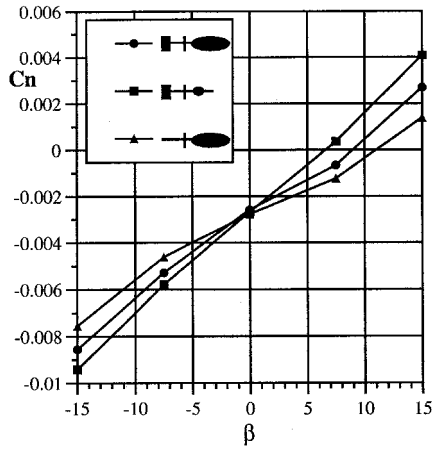

Fig. 12 Effect of configuration on *Cn* (α = 0).

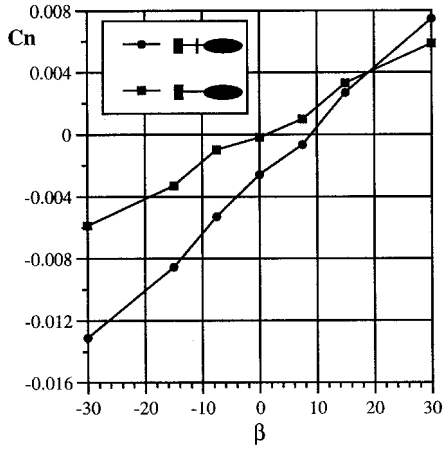

Fig. 13 Effect of power on *Cn* (α = 0).

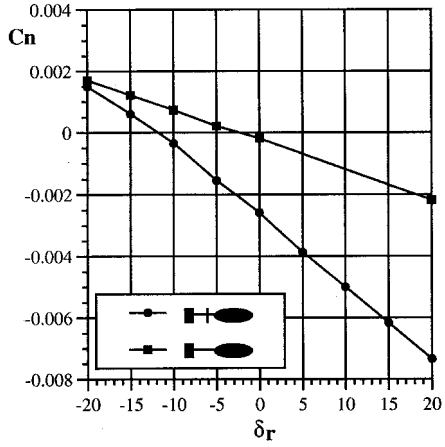

Fig. 14 Effect of power setting on rudder effectiveness (α = 0, β = 0).

and so gives a near constant offset to the curve. For this particular vehicle, the additional side force at the tail acts to reduce the yawing moment.

Rudder Effectiveness

The most significant effects of the rudder are on the side force and yawing moments. It was found that the rudder effect on both side force and yawing moment was almost linear at a given α, regardless of the power setting. This is illustrated in Fig. 14, where the effect of rudder setting on *Cn* at zero incidence and sideslip is compared for power-on and power-off modes. Note that in the power-off mode, data were only measured for negative δ_r and at δ_r = 20 deg. Intermediate points are, therefore, interpolated for illustrative purposes.

It may be observed that the effect of power is to substantially increase the gradient of the yawing moment curve. As discussed previously, both the rotational and increased axial velocities, produced by the propeller, influence the performance of the vertical tail surfaces. The net result of power in this particular case is to almost double the gradient of the curve and, hence, the rudder effectiveness.

As in the case of the vertical tail, the enhanced performance of the rudder, as a result of the propwash, diminishes as the angle of attack of the gyroplane increases and the tail moves into clear air. In fact, regardless of power setting, the rudder effectiveness reduces at high α because of the strongly three-dimensional flow around the tail surfaces.

The only other significant effect of the rudder arises from the displacement of its c.p. from the c.m. This produces a slight rolling moment when the rudder is deflected.

Concluding Remarks

The aerodynamic characteristics of the gyroplane configurations considered in this study are generally benign. It is, however, pertinent to note that there are several effects associated with the cowling that are detrimental to stability. Although the cowling on the test model was particularly large, it is likely that any open cowling design will be subject to similar effects. Additionally, the length of the cowling used in this study is substantial; extending from well in front of the pilot up to the rotor support column. The increased wetted area this presents to the onset flow in sideslip acts to oppose the stabilizing effect of the tail. The tail itself benefits from the additional side force produced by the end plates on the horizontal surfaces.

Acknowledgments

This work was supported by the U.K. Civil Aviation Authority, under Contract 7D/S/1125 Aerodynamics of Gyroplanes. The authors also wish to acknowledge the contributions to the project of R. Galbraith and S. Houston of Glasgow University, and M. Holl of VZLU. Presented as Paper 96-4.3.4 at the 20th Congress of the International Council of the Aeronautical Sciences, Sorrento, Italy, Sept. 8–13, 1996.

References

[1]Anon., "Airworthiness Review of Air Command Ggyroplanes," U.K. Civil Aviation Authority Air Accidents Investigation Branch Rept., Sept. 1991.

[2]McKillip, R. M., and Chih, M. H., "Instrumented Blade Experiments Using a Light Autogyro," *Proceedings of the 16th European Rotorcraft Forum*, Vol. 2, The Royal Aeronautical Society, London, 1990, pp. 8.4.1–8.4.8.

[3]Glauert, H., "A General Theory of the Autogyro," Aeronautical Research Committee, R&M 1111, Nov. 1926.

[4]Lock, C. N. H., "Further Development of Autogyro Theory Parts I and II," Aeronautical Research Committee, R&M 1127, March 1927.

[5]Glauert, H., "Lift and Torque of an Autogyro on the Ground," Aeronautical Research Committee, R&M 1131, July 1927.

[6]Lock, C. N. H., and Townend, H. C. H., "Wind Tunnel Experiments on a Model Autogyro at Small Angles of Incidence," Aeronautical Research Committee, R&M 1154, March 1927.

[7]Glauert, H., and Lock, C. N. H., "A Summary of the Experimental and Theoretical Investigations of the Characteristics of an Autogyro," Aeronautical Research Committee, R&M 1162, April 1928.

[8]Wheatly, J. B., "Wing Pressure Distribution and Rotor Blade Motion of an Autogyro as Determined in Flight," NACA TR 475, Jan. 1933.

[9]Wheatly, J. B., "An Aerodynamic Analysis of the Autogyro Rotor with a Comparison Between Calculated and Experimental Results," NACA TR-487, Jan. 1934.

[10]Wheatly, J. B., and Hood, M. J., "Full-Scale Wind-Tunnel Tests of a PCA-2 Autogyro Rotor," NACA TR 515, Jan. 1935.

[11]Wheatly, J. B., "An Analytical and Experimental Study of the Effect of Periodic Blade Twist on the Thrust, Torque and Flapping Motion of an Autogyro Rotor," NACA TR 591, Jan. 1937.

[12]Anon, "British Civil Airworthiness Requirements Section T: Light Gyroplane Design Requirements," U.K. Civil Aviation Authority, Paper T860, July 1993.

[13]Houston, S. S., "Longitudinal Stability of Gyroplanes," *The Aeronautical Journal*, Vol. 100, No. 991, 1996, pp. 1–6.